

MIPP Momentum resolution and acceptances

Rajendran Raja^{1,*}

¹*Fermi National Accelerator Laboratory,*

P. O. Box 500, Batavia, IL 60510

(Dated: November 30, 2007)

Abstract

We describe the process by which acceptances and resolutions are calculated for MIPP.

*Electronic address: raja@fnal.gov

I. INTRODUCTION

We describe an analysis of MIPP Monte Carlo events generated on the liquid hydrogen target using DPMJet using 6 beam species (π^\pm , K^\pm and p^\pm) at beam momenta 19 GeV/c, 58 GeV/c and 85 GeV/c. There were 10,000 events generated for each beam species at a given momentum, yielding a sample of 180,000 events that were sent through the Monte Carlo and reconstruction programs.

II. MATCHING MONTE CARLO AND RECONSTRUCTED TRACKS

A module MCMatch was written, that resides in the library MCTruth that matches MC (Class MCCParticle) and Reco (Class RBKTrack) tracks. The algorithm may be described as follows. We demand that the charges of reco and MC tracks match and that the vertex of the MC track lie within $-10.0 < V_x < 10.0$, $-10.0 < V_y < 10.0$, $-10.0 < V_z < 10.0$, $-840.0 < V_z < -676.0$ for this analysis. The last cut includes tracks generated within the upstream 3/4 of the TPC volume and includes all tracks originating from the liquid Hydrogen target flask. The same vertex selection is made for the Reco track candidates to match.

In the first pass, none of the momentum and resolution functions are known. So we work out the least square of the vector three momentum difference $lsq = |\vec{p}_{reco} - \vec{p}_{MC}|^2$ between the reco and MC track candidates for all track pairs that satisfy the vertex and charge criteria.

The track pairs are then sorted by lsq and the ambiguities eliminated by confirming matches of pairs starting with the lowest lsq . This process yields three classes of tracks-

- MC tracks which possess Reco track matches. (Class Matches)
- MC tracks which do not possess Reco track matches(class Nomatch_MC).
- Reco tracks that do not possess corresponding MC tracks matches (class Nomatch_RBK). This last item is due to spurious track finding problems and needs to be investigated algorithmically.

III. MOMENTUM RESOLUTION

We divide the matched secondary tracks according to MC momentum bins delineated by (0,1.0,5.0,10.0,20.0,30.0,40.0,50.0,70.0,90.0) GeV/c and histogram dp , the difference between the reconstructed momentum and the MC momentum. We fit this histogram to a double Gaussian as shown in Fig. 1.

Figure 2 shows the MIPP fractional momentum resolution thus evaluated for matched tracks as a function of track momentum. The fitted curve is used to produce a function $mipp_dp(p)$ which gives the expected momentum resolution for an MC track of momentum p .

IV. ANGULAR RESOLUTION

In order to form a better matching algorithm, we need not only the resolution in momentum but also the angular resolution of the tracks. We study the angles $a_x = p_x/p$ and $a_y = p_y/p$ and evaluate da_x and da_y the differences in a_x , a_y between reco and MC tracks as a function of momentum in the same momentum ranges as for the momentum resolution study. Figure 3 shows the overall distribution of da_x and the scatter plot of da_x as a function of momentum \times charge of the track.. The effects of multiple scattering is evident as one approaches lower momentum, since values of da_x increase dramatically. Fig 4 shows a similar set of plots for da_y . We work out the resolutions in a_x and a_y using a similar fitting technique to the one used for momentum resolutions. Figure 5 shows the resolutions in a_x and a_y thus obtained. The angular resolutions are then obtained for any given track using linear interpolation in the routines $mipp_ax(p)$ and $mipp_ay(p)$. These resolutions are then employed to obtain a matching χ^2 between reco and MC tracks for the three quantities da_x , da_y and dp . Figure 6 shows the distribution of the overall χ^2 and the individual χ^2 in the three components. Figure 7 upper plot shows the distribution of $\chi_p = dp/\sigma(p)$, the (difference in reco and MC momenta)/momentum resolution. Fig 7 lower plot shows the distribution of χ_p as a function of momentum*charge of the MC track.

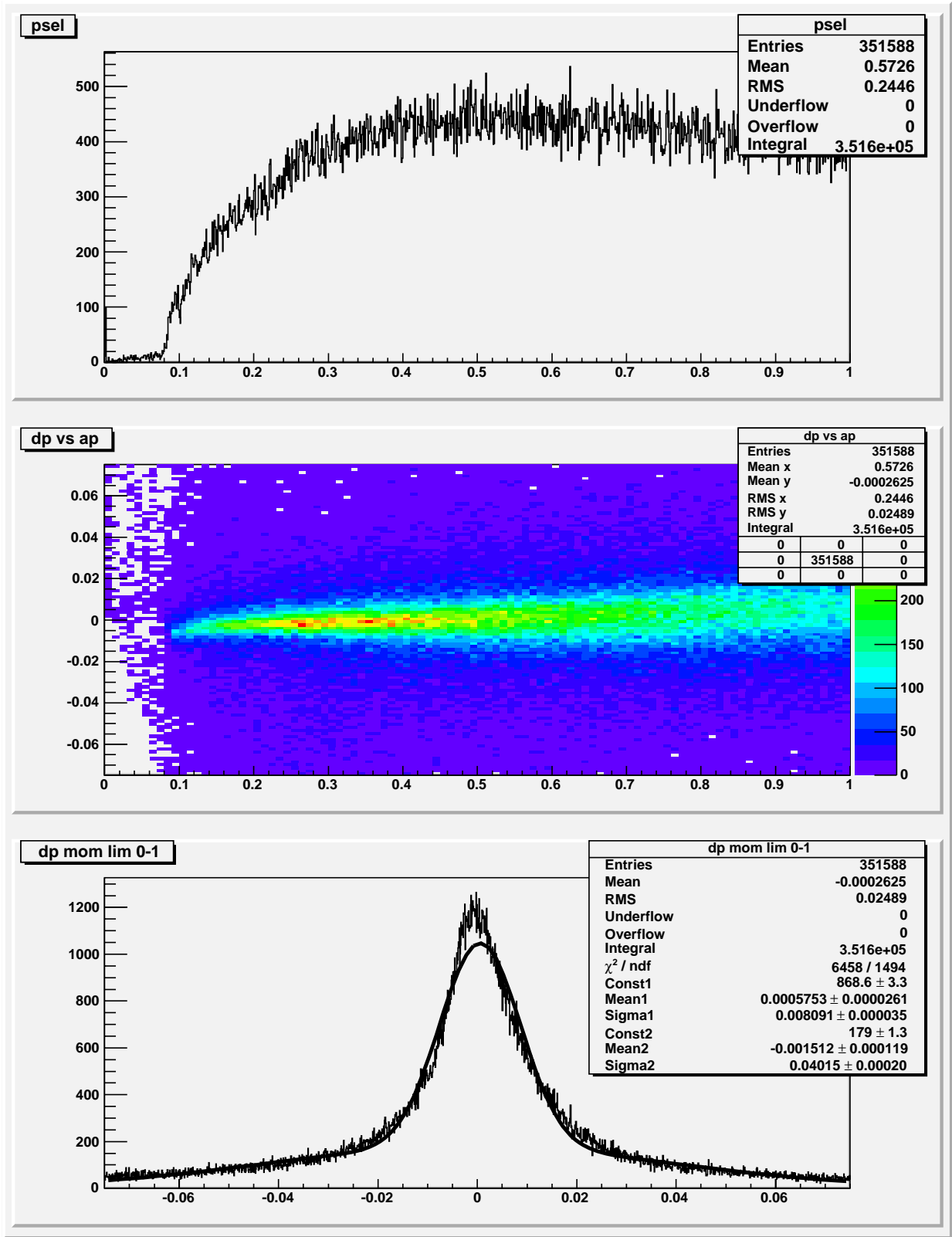


FIG. 1: Top histogram shows the momentum spectrum of secondary tracks in the range 0-1.0GeV/c. The middle histogram shows the scatter plot of dp , the difference between reco and MC momentum as a function of momentum and the bottom histogram shows the histogram of dp in this momentum range. A fit to a double Gaussian is shown.

HARP MIPP Resolution Comparison

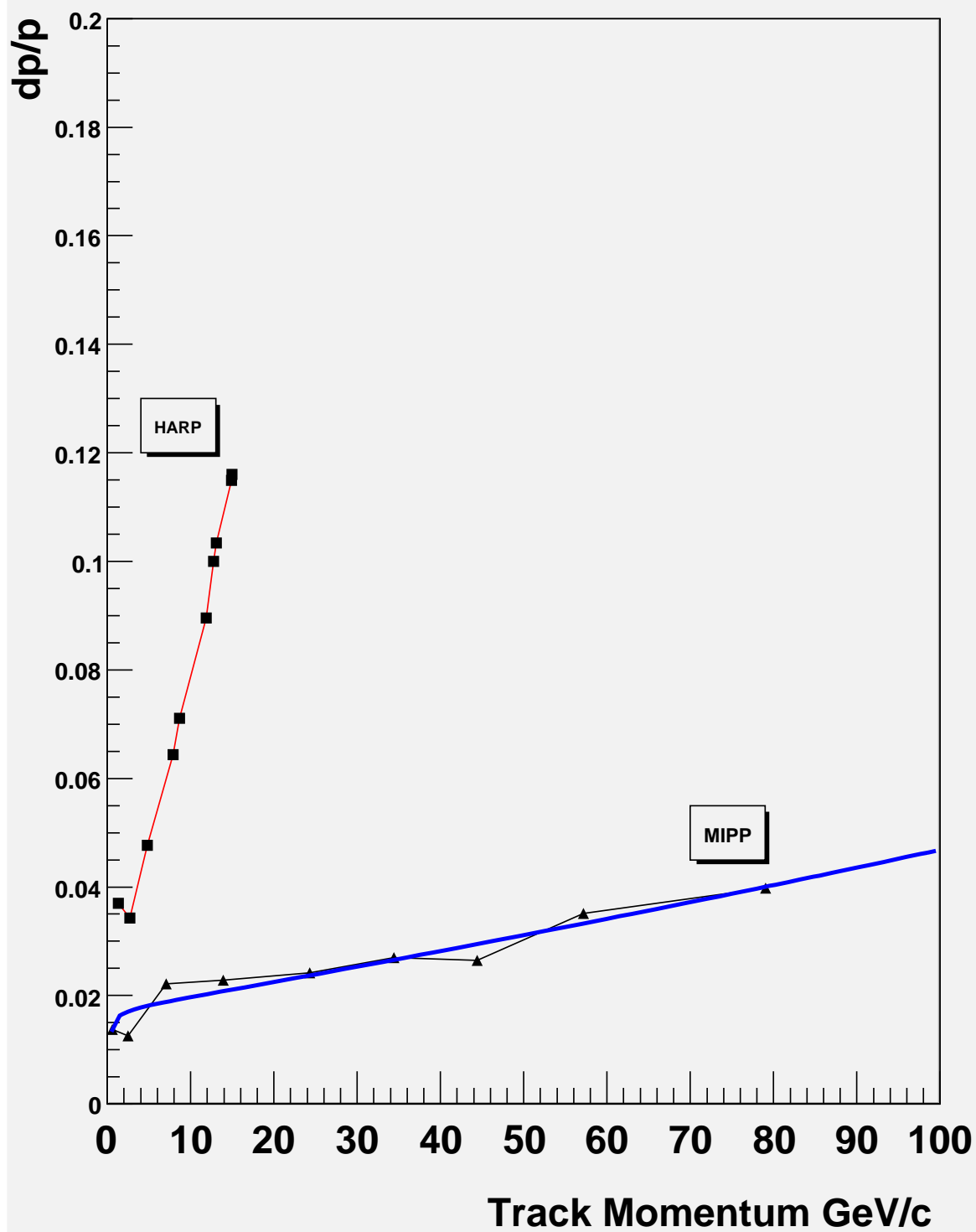


FIG. 2: The MIPP fractional momentum resolution dp/p as a function of MC momentum. The HARP published resolution is shown for comparison.

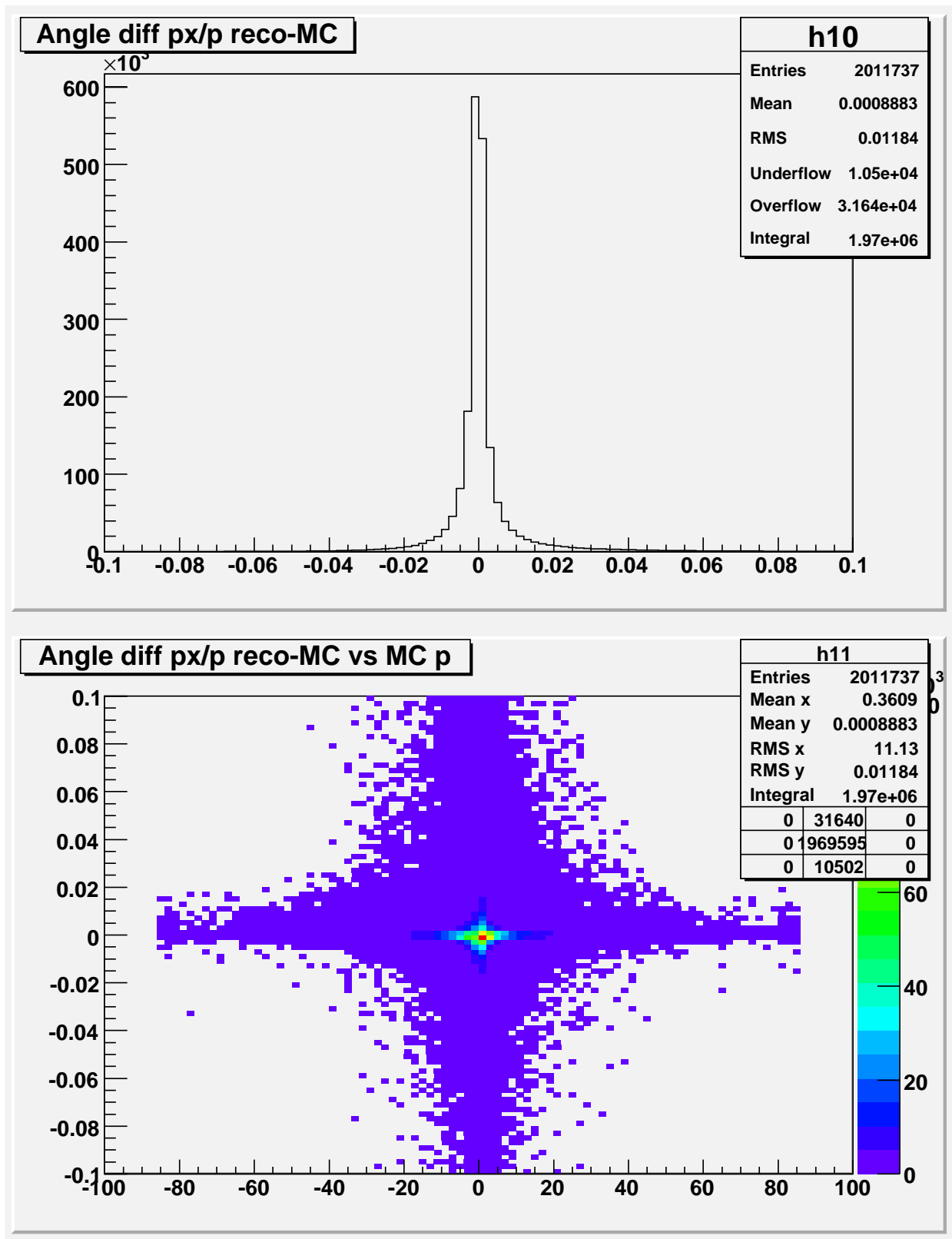


FIG. 3: The top plot shows the histogram of da_x the difference between reco and MC of the quantity p_x/p for all matched tracks. The bottom plot is the scatter plot of da_x vs momentum \times charge of the MC track. The effects of multiple scattering are evident as one goes towards smaller momenta.

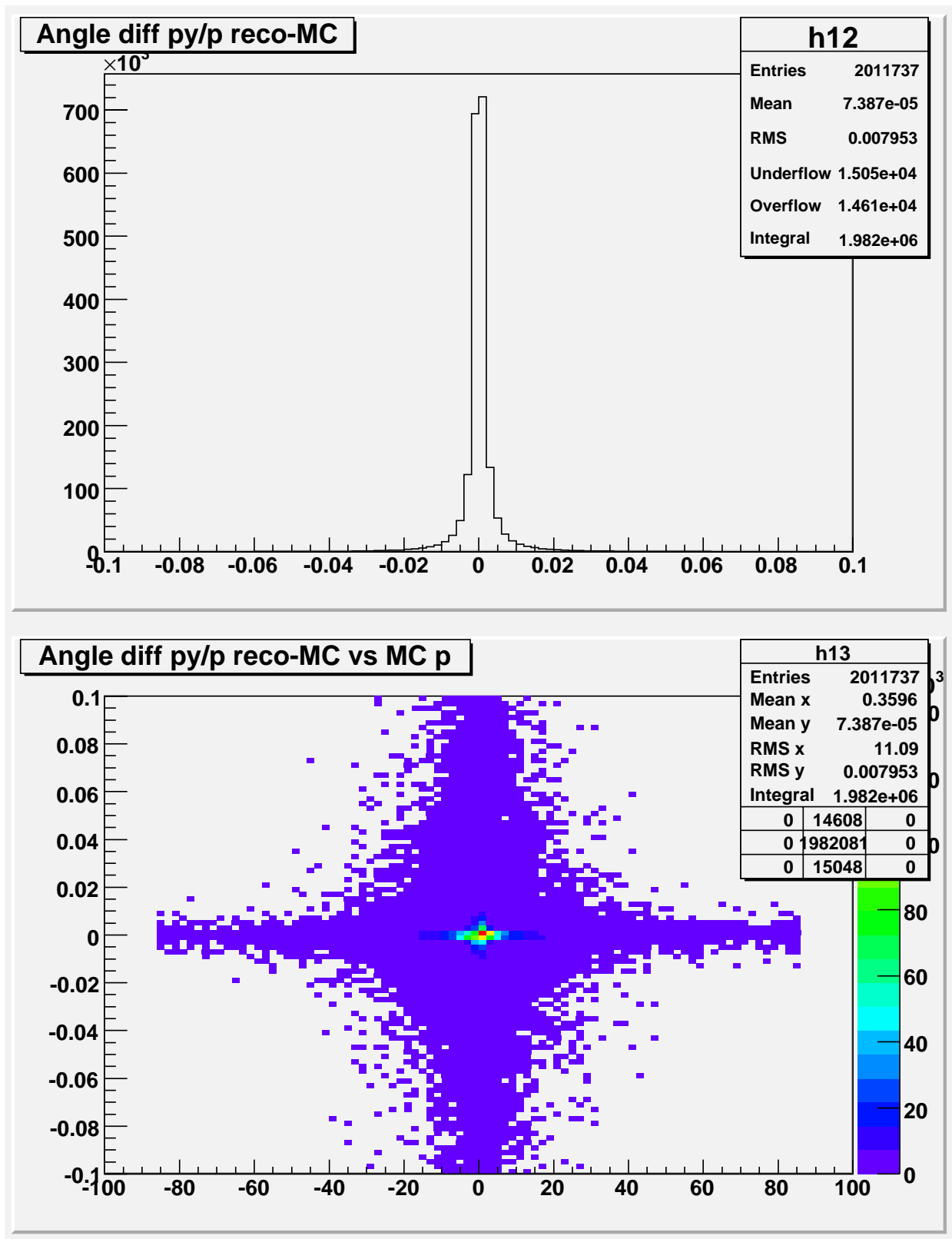


FIG. 4: The top plot shows the histogram of da_y the difference between reco and MC of the quantity p_y/p for all matched tracks. The bottom plot is the scatter plot of da_y vs momentum \times charge of the MC track. The effects of multiple scattering are evident as one goes towards smaller momenta.

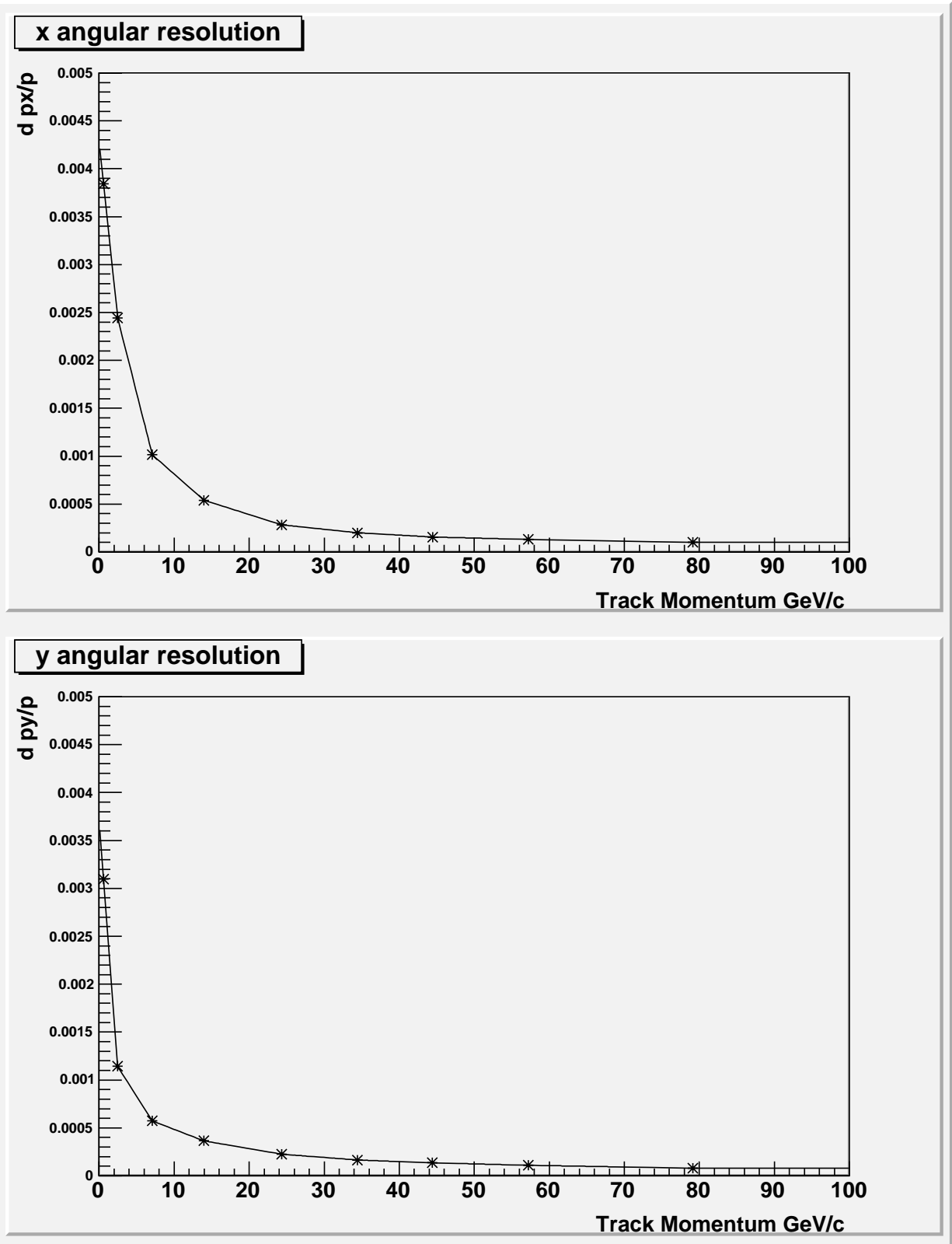


FIG. 5: The top plot shows the fitted resolution in a_x , the difference in p_x/p as a function of the MC momentum of the track. The bottom plot shows the resolution in $a_y = p_y/p$.

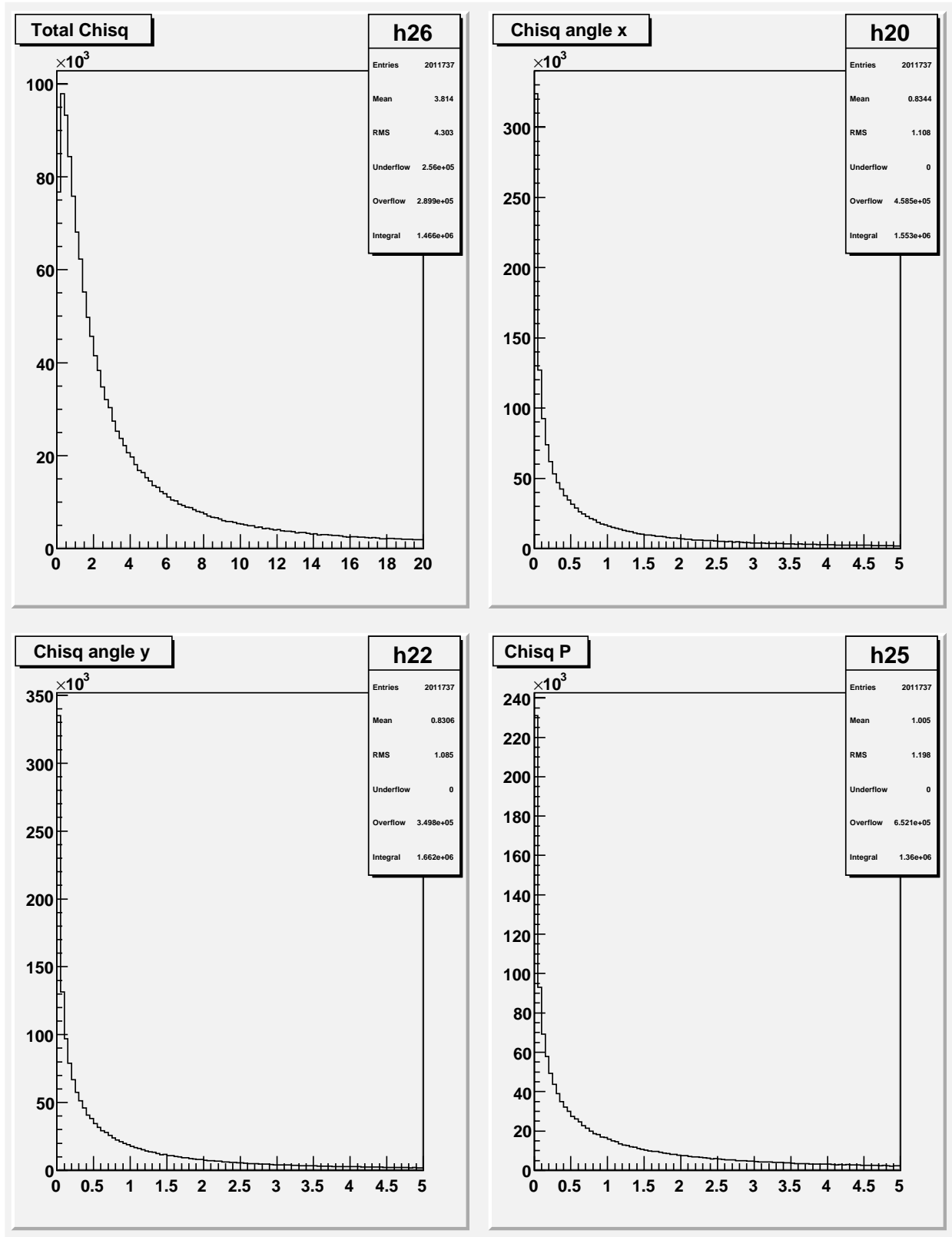


FIG. 6: Upper left shows the overall χ^2 distribution. Upper right shows the χ^2 contribution from a_x . The lower plots show the χ^2 contributions from a_y and p .

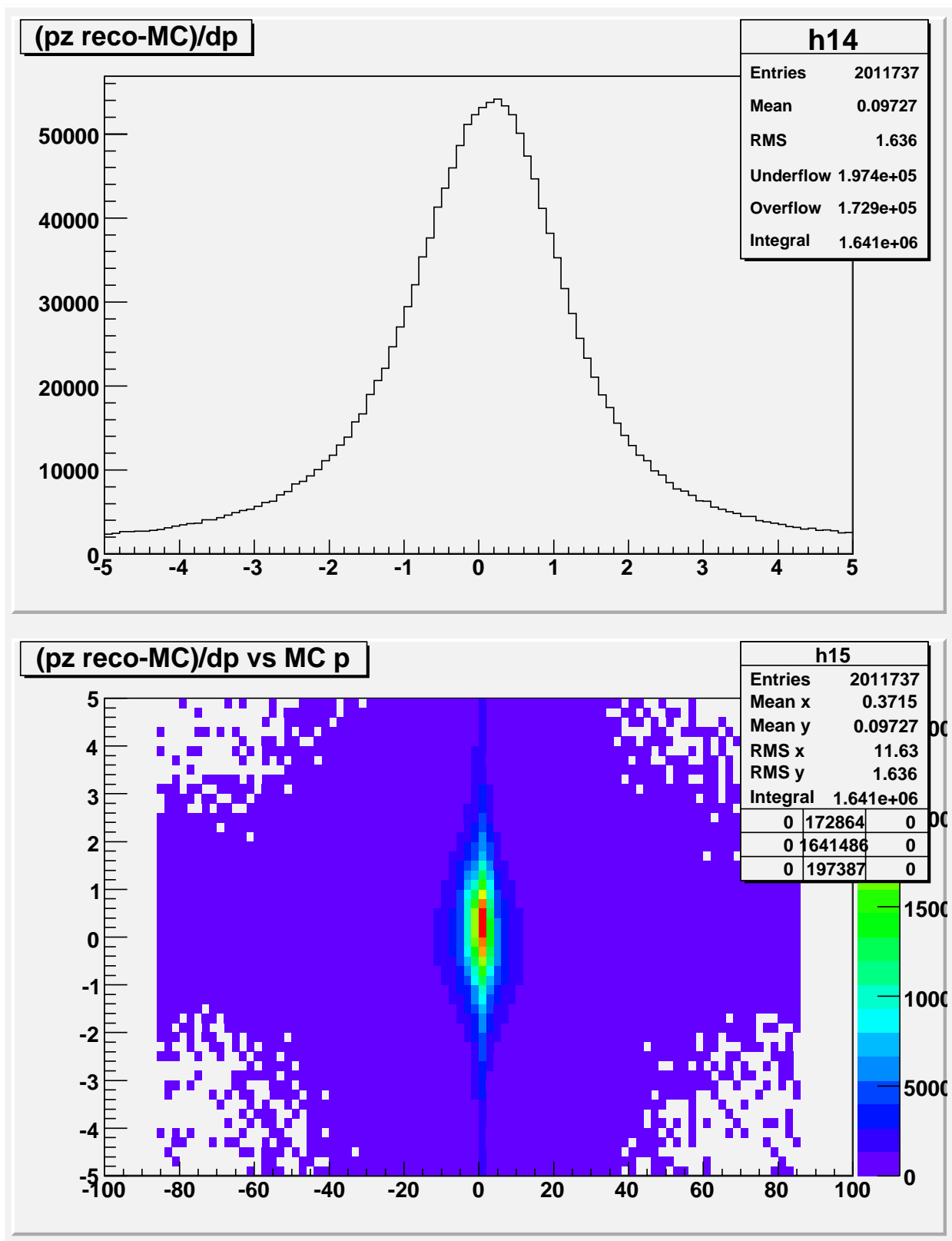


FIG. 7: The top plot shows the distribution for $\chi_p = dp/\sigma(p)$, where dp is the difference between reco and MC momentum. The bottom scatter plot shows the distribution of χ_p as a function of momentum \times charge of the MC track.

V. SECOND ITERATION OF MATCHING

We now do a second iteration of the matching algorithm and use the χ^2 instead of the momentum least squares for the matching determinant. Figure 8 shows the distribution of the overall χ^2 and the integral distribution of the χ^2 . It can be seen that a cut of $\chi^2 = 200$ has an efficiency of keeping $\approx 95\%$ of the matched tracks. Applying this cut to the matched data produces the plots shown in Figure 9 where the distributions in angle are considerably tidied up (perhaps too much so).

VI. CALCULATION OF ACCEPTANCES AND EFFICIENCIES

We now have all the tools to calculate acceptances and efficiencies. Figure 10 top left plot shows the scatter plot of momentum vs the polar angle θ wrt the z axis along the beam direction for tracks which match. The top right hand plot shows the same plot for tracks for which a reco candidate was found but for which there is no MC track to match. The middle left plot shows the scatter for MC tracks for which no reco track was found to match. The middle right hand plot shows the efficiency as a function of momentum and θ . The bottom plots show the efficiency as a function of momentum and θ respectively. It can be seen that the overall acceptance \times track finding efficiency is of the order of 95% irrespective of momentum. For tracks at large angles of θ , there is a loss of efficiency due to smaller track lengths in the TPC.

Figure 11 shows the same plot as in Figure 10 but with a cut of $\chi^2 < 200$ imposed. It can be seen that this cut selectively cuts out events with small momentum at large values of θ . This is where multiple scattering is predominant and one can expect significant deviation from Gaussian behavior. We thus decide not to employ scattering χ^2 cut but only use the χ^2 for ordering the track matches to obtain the best matches.

We now look at some distributions for 85 GeV/c beam momentum, combining the beam species. Figure 12 shows the acceptance \times efficiency for all particles in center of mass rapidity. There is clearly loss of particles in the backward cms hemisphere due to wide angle tracks missing the TPC. Figure 13 shows the acceptance \times efficiency for all particles in Feynman x . This variable is particularly sensitive to the mass of the particle which explains the shape of the acceptance when summed over particle species. This dependence is seen more clearly

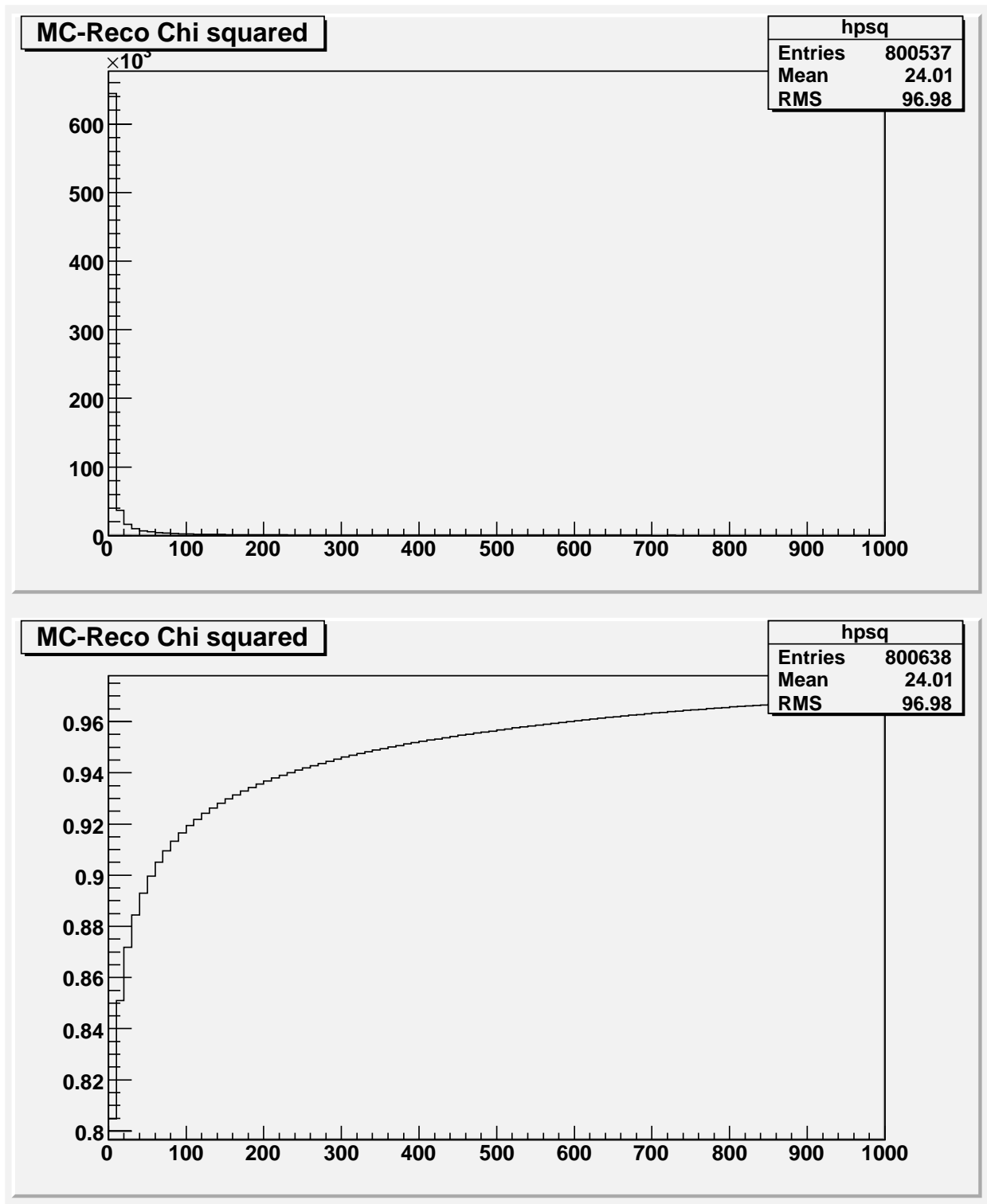


FIG. 8: The three component distributions for da_x , da_y and dp as a function of momentum*charge of the MC track after an overall cut of $\chi^2 < 200$ was applied to the matched sample. Compare to the distributions with no cut in Figures 3 and 4.

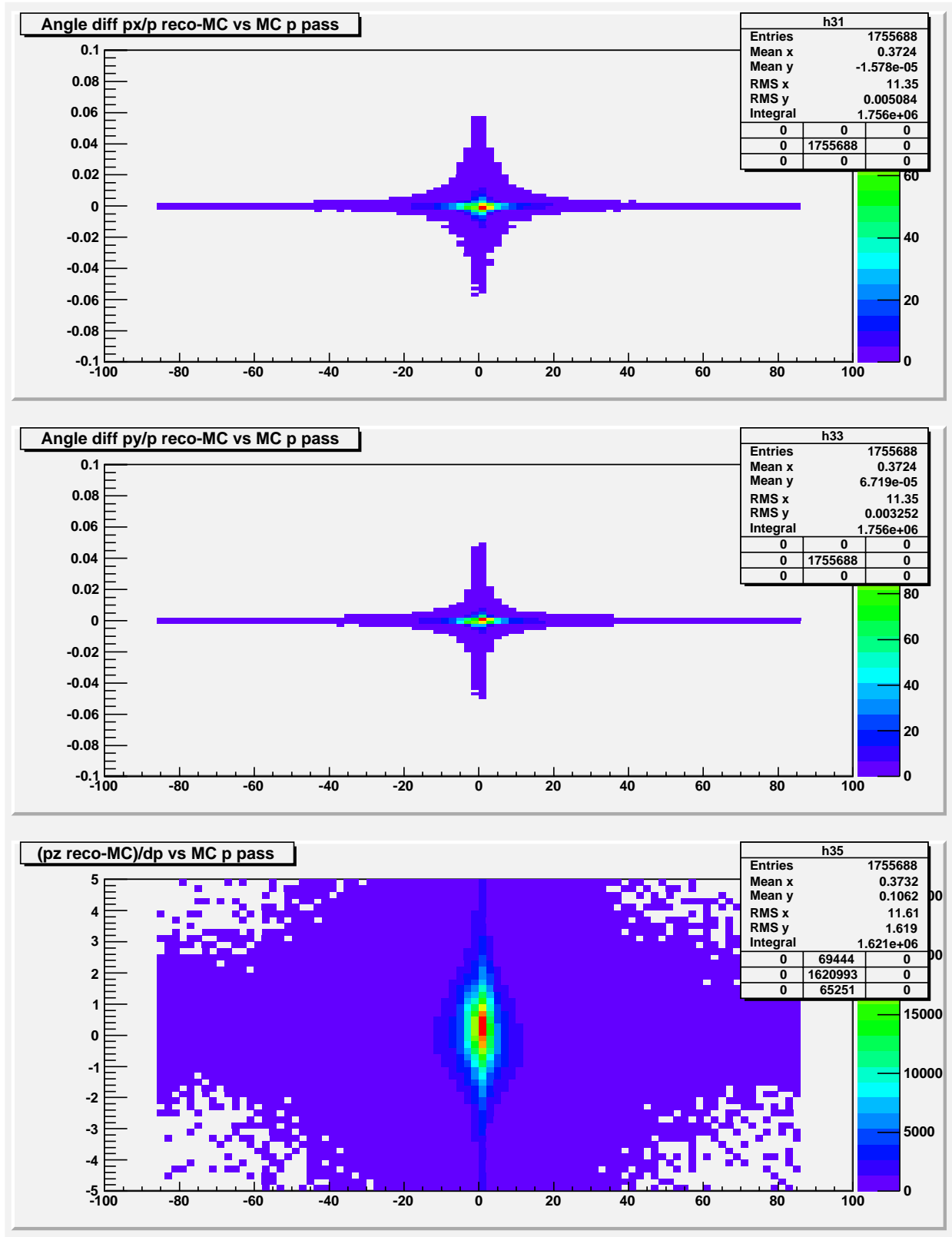


FIG. 9: The distributions in da_x , da_y and χ_p as a function of momentum \times charge of the MC track after applying a $\chi^2 < 200$ cut. Compare with Figures 3 and 4 7 which show the same quantities before the cut.

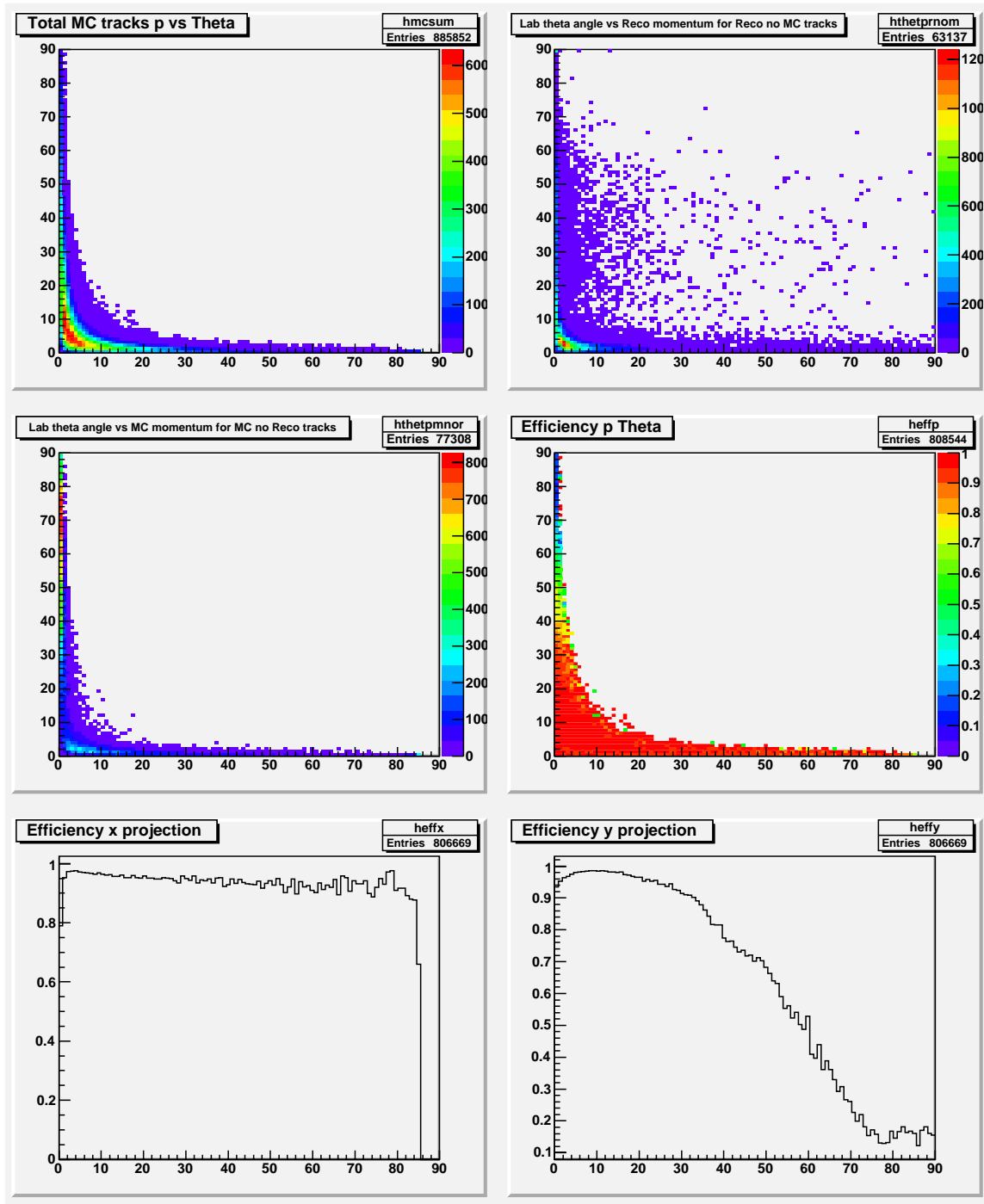


FIG. 10: Top left-Histogram of MC momentum p vs θ for matching tracks. Top right- for Reco tracks that have no MC partner. middle-left-For MC tracks that have no Reco partner. Middle right-Acceptance \times Efficiency in p, θ . Bottom left, acceptance \times efficiency as a function of p and bottom right as a function of θ . No χ^2 cut employed.

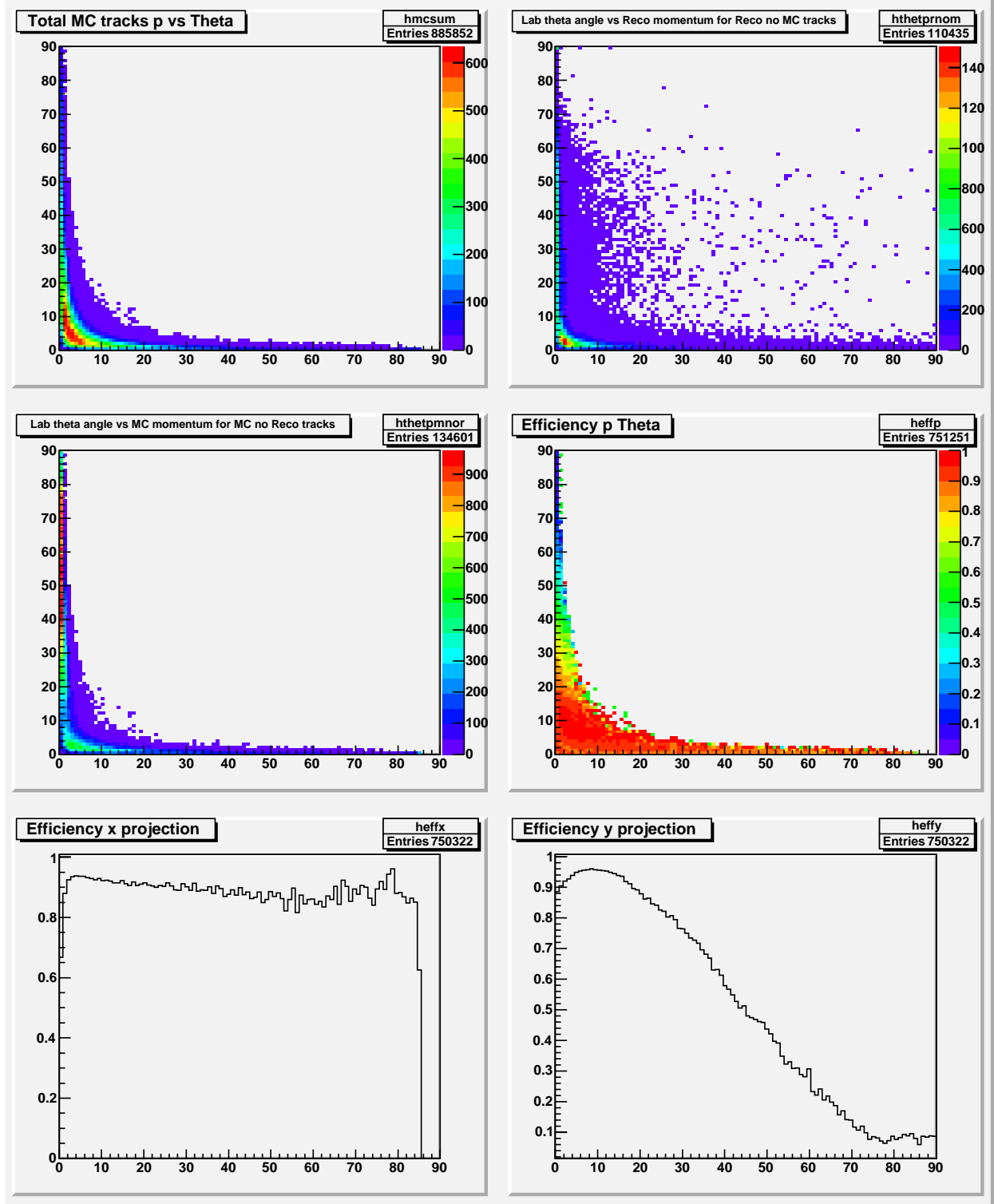


FIG. 11: Top left-Histogram of MC momentum p vs θ for matching tracks. Top right- for Reco tracks that have no MC partner. middle-left-For MC tracks that have no Reco partner. Middle right-Acceptance \times Efficiency in p, θ . Bottom left, acceptance \times efficiency as a function of p and bottom right as a function of θ . $\chi^2 < 200$ cut employed.

in Figures 14,15and 16 which show the Feynman X acceptance \times efficiency for pions, kaons and protons respectively.

VII. CONCLUSION

MIPP has excellent acceptances and resolutions. We will put this to good use when publishing cross sections.

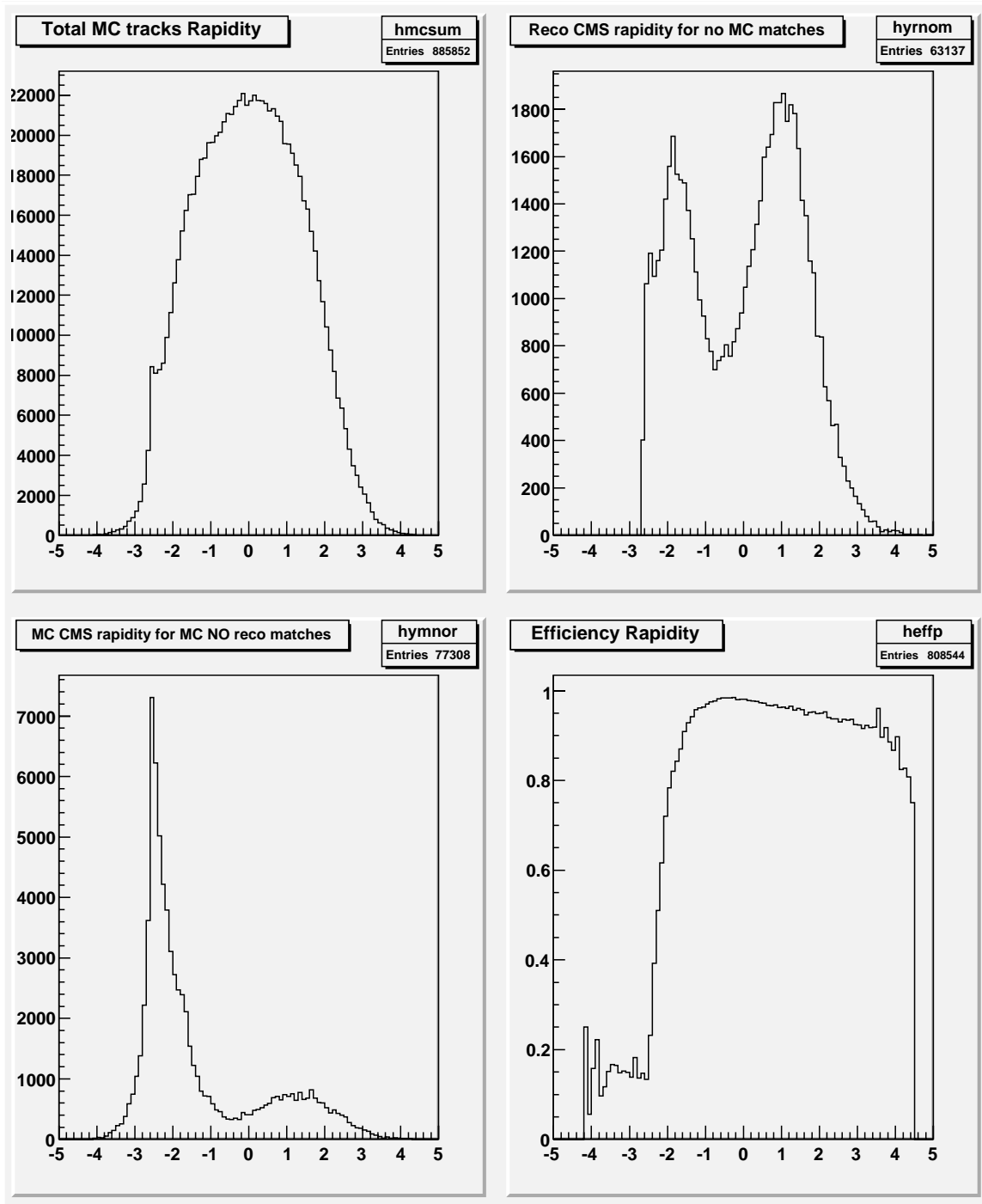


FIG. 12: Acceptance \times Efficiency in cms rapidity for all particles. The top left plot shows MC-reco matches. The top right is for reco tracks with no MC matches and the bottom left shows the MC tracks with no reco matches. The bottom right plot shows the Acceptance \times efficiency.

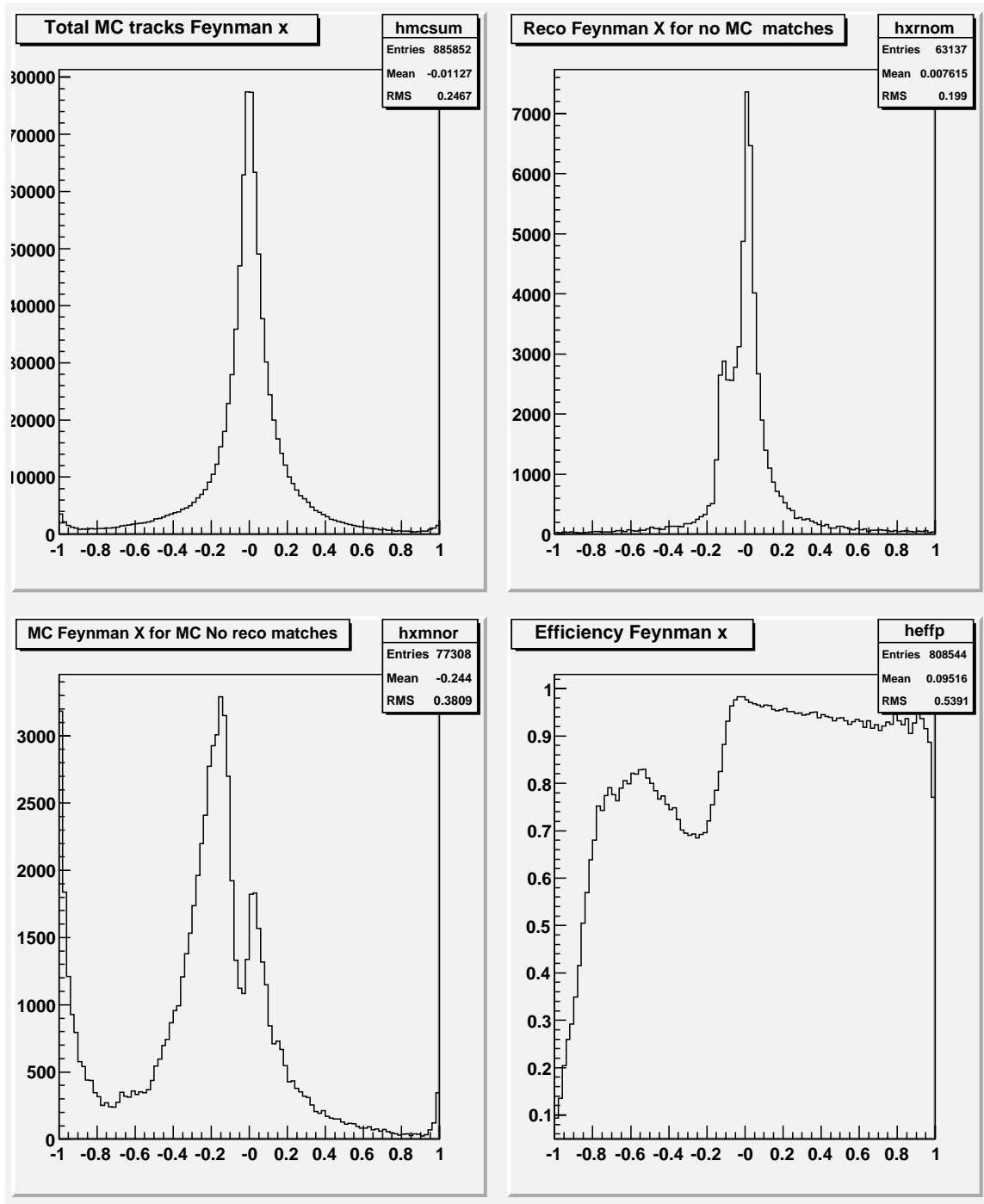


FIG. 13: Acceptance \times Efficiency in Feynman x for all particles. The top left plot shows MC-reco matches. The top right is for reco tracks with no MC matches and the bottom left shows the MC tracks with no reco matches. The bottom right plot shows the Acceptance \times efficiency.

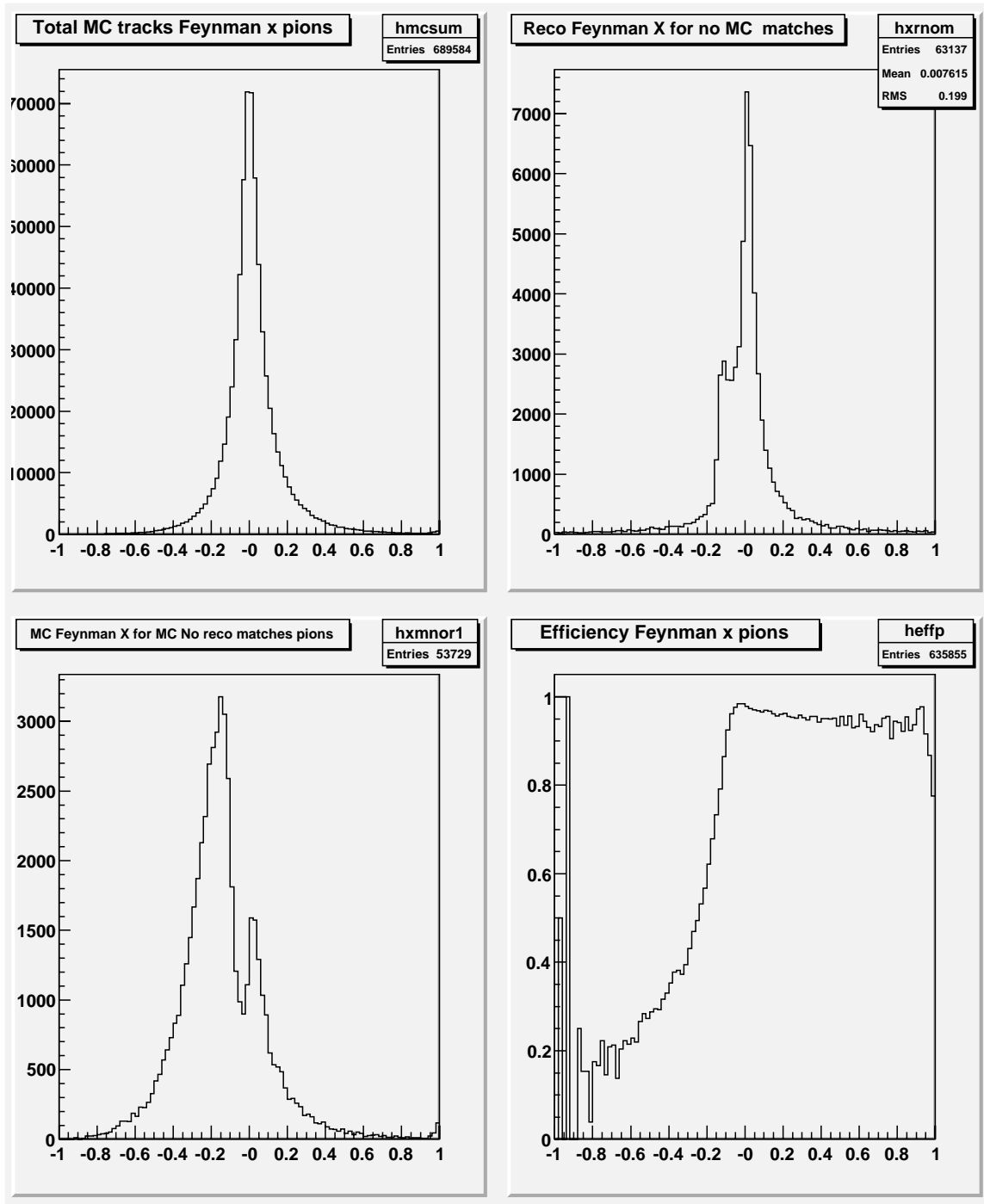


FIG. 14: Acceptance \times Efficiency in Feynman x for all pions. The top left plot shows MC-reco matches. The top right is for reco tracks with no MC matches and the bottom left shows the MC tracks with no reco matches. The bottom right plot shows the Acceptance \times efficiency.

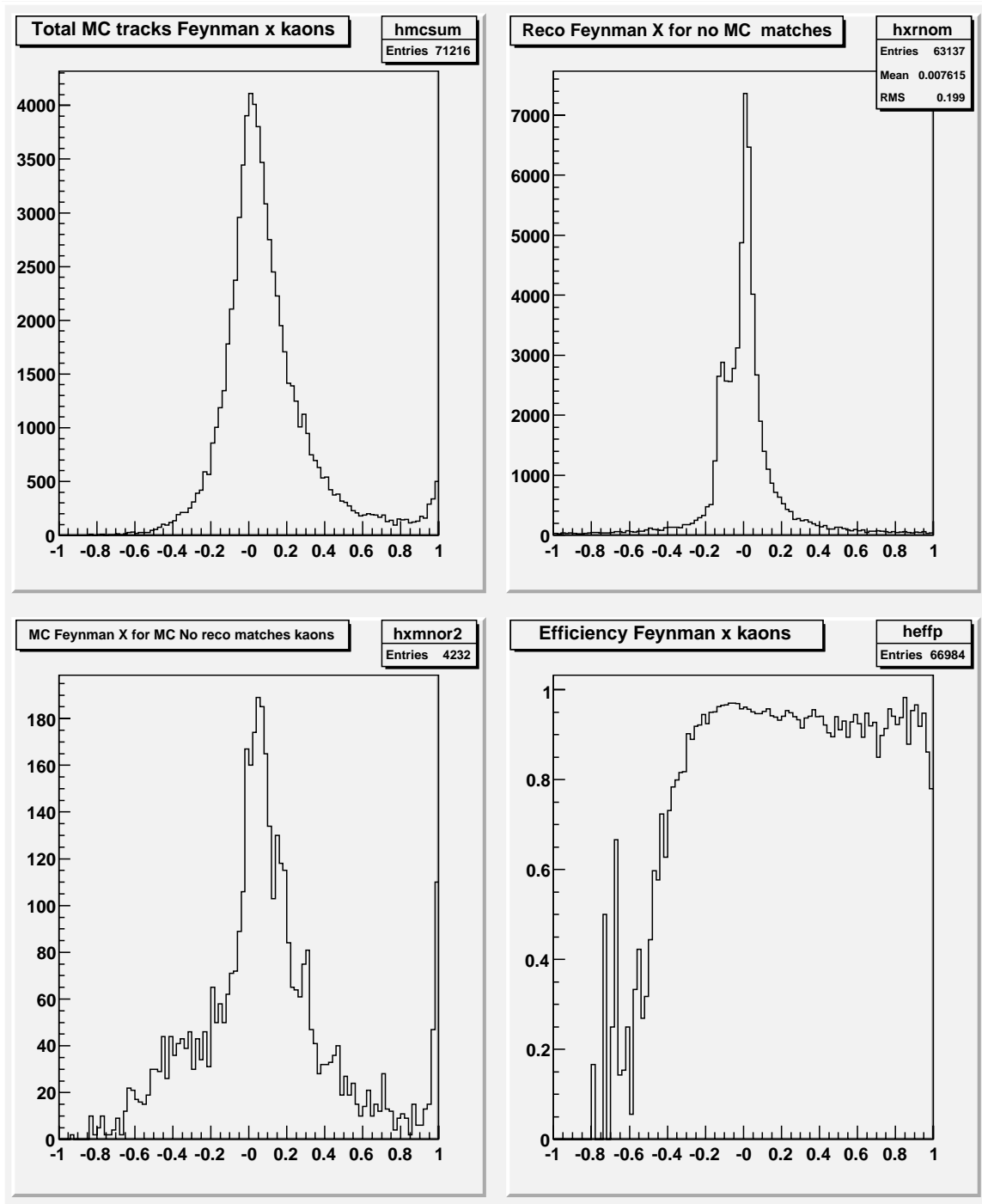


FIG. 15: Acceptance \times Efficiency in Feynman x for kaons. The top left plot shows MC-reco matches. The top right is for reco tracks with no MC matches and the bottom left shows the MC tracks with no reco matches. The bottom right plot shows the Acceptance \times efficiency.

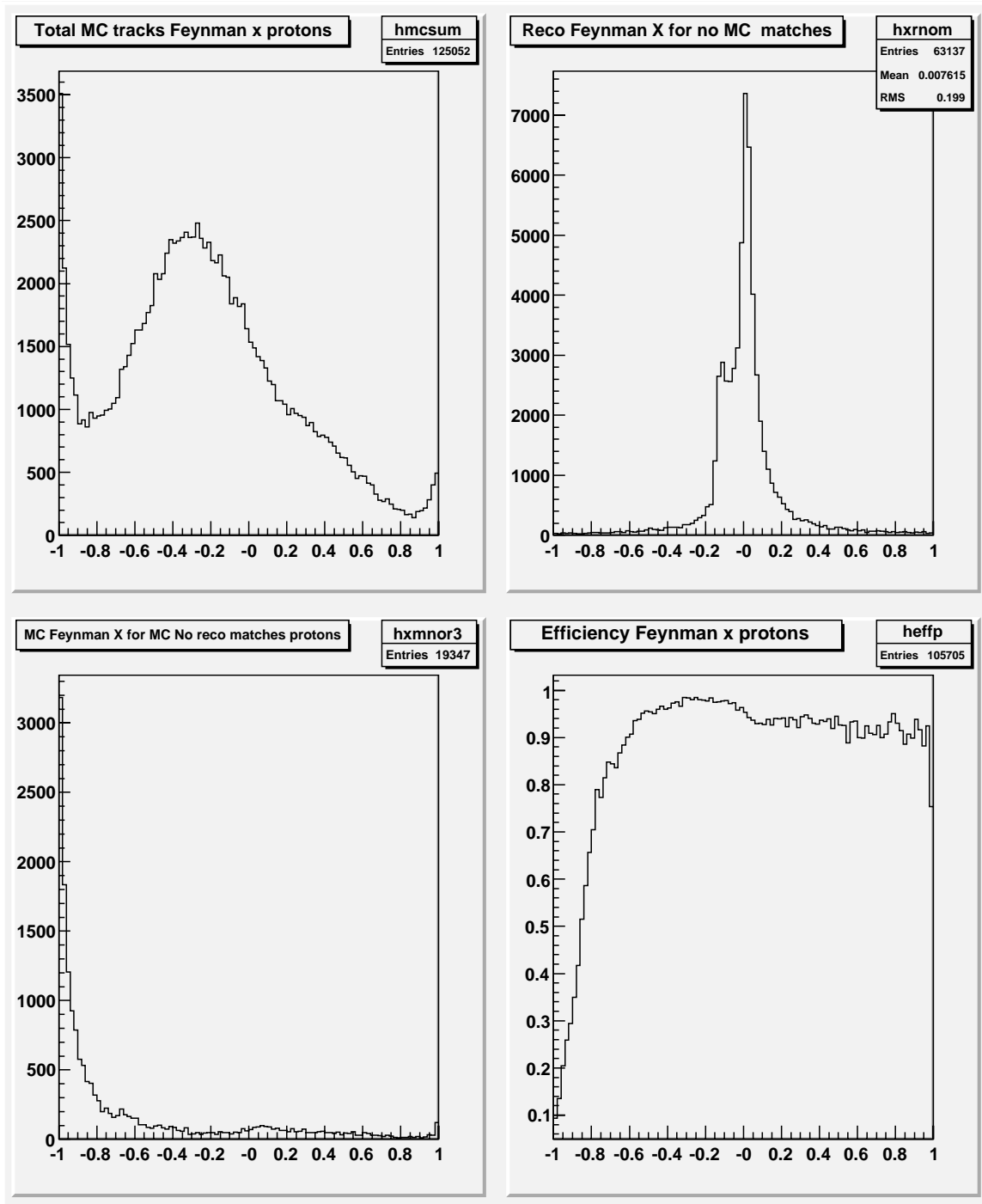


FIG. 16: Acceptance \times Efficiency in Feynman x for all protons. The top left plot shows MC-reco matches. The top right is for reco tracks with no MC matches and the bottom left shows the MC tracks with no reco matches. The bottom right plot shows the Acceptance \times efficiency.